

To appear in The Astrophysical Journal

## Dense Gas in the Milky Way

Tamara T. Helfer<sup>1</sup> and Leo Blitz<sup>1</sup>

Department of Astronomy, University of Maryland, College Park, MD 20742

### ABSTRACT

We present a study of dense gas emission in the Milky Way in order to serve as a basis for comparison with extragalactic results. This study combines new observations of HCN, CS, and CO in individual GMCs and in the Milky Way plane with published studies of emission from these molecules in the inner 500 pc of the Milky Way. We find a strong trend in the fraction of emission from dense gas tracers as a function of location in the Milky Way: in the bulge,  $I_{\text{HCN}}/I_{\text{CO}} = 0.081 \pm 0.004$ , in the plane,  $I_{\text{HCN}}/I_{\text{CO}} = 0.026 \pm 0.008$  on average, and over the full extent of nearby GMCs,  $I_{\text{HCN}}/I_{\text{CO}} = 0.014 \pm 0.020$ . Similar trends are seen in  $I_{\text{CS}}/I_{\text{CO}}$ : in the bulge,  $I_{\text{CS}}/I_{\text{CO}} = 0.027 \pm 0.006$ , in the plane,  $I_{\text{CS}}/I_{\text{CO}} = 0.018 \pm 0.008$  on average, and over the full extent of nearby GMCs,  $I_{\text{CS}}/I_{\text{CO}} = 0.013 \pm 0.02$ . The low intensities of the HCN and CS emission in the plane suggests that these lines are produced by gas at moderate densities; they are thus not like the emission produced by the dense, pc-scale star forming cores in nearby GMCs. The contrast between the bulge and disk ratios in the Milky Way is likely to be caused by a combination of higher kinetic temperatures as well as a higher dense gas fraction in the bulge of the Milky Way. We show that the ratio  $I_{\text{HCN}}/I_{\text{CO}}$  is correlated quantitatively with the total hydrostatic gas pressure in the Milky Way as  $I_{\text{HCN}}/I_{\text{CO}} \propto P^{0.19 \pm 0.04}$ .

*Subject headings:* galaxy:general—galaxy:structure—ISM:general—  
ISM:molecules—ISM:structure

---

<sup>1</sup>thelfer,blitz@astro.berkeley.edu, current address Radio Astronomy Lab, 601 Campbell Hall, UC Berkeley, Berkeley CA 94720

## 1. Introduction

Any study of extragalactic phenomena demands a comparison with conditions in the Milky Way, which in the absence of compelling contradictions is used as a reference for what is “normal” in a spiral galaxy. The result that the centers of most nearby spiral galaxies contain a large amount of gas at densities of  $\sim 10^5 \text{ cm}^{-3}$  (traced by HCN and CS emission, Nguyen-Q-Rieu et al. 1992; Helfer & Blitz 1993) is surprising when compared to conditions in giant molecular clouds (GMCs) in the solar neighborhood, where typical clump densities are only  $\sim 10^{2.5} - 10^{3.5} \text{ cm}^{-3}$  (Blitz 1987) and which contain relatively few clumps of dense gas emission (e.g. Lada, Bally, & Stark 1991). What is questionable, however, is how meaningful such a comparison between the centers of galaxies and the local environment of the Sun is to the interpretation of the HCN and CS observations. The goal of this paper is to investigate the properties of GMCs as a function of their location within the Milky Way: do GMCs within the high-pressure environment of the Galactic bulge have the same physical properties as GMCs in the Galactic disk and near the Sun? Throughout this study, we use as a qualitative indicator of pressure the ratios of the 3 mm emission from the dense gas tracers HCN and CS relative to that of CO. (HCN and CS typically trace gas densities of  $10^5 \text{ cm}^{-3}$  or higher; this is about 100 times the critical density required to excite CO.)

In the Milky Way, emission from dense molecular gas tracers has been studied in the bulge (CS: Bally et al. 1987; HCN: Jackson et al. 1996), where it is distributed over a size scale of  $d \sim 500 \text{ pc}$ , and in many individual star-forming cores in nearby GMCs, on size scales of a few pc or smaller. To complicate extragalactic comparisons with the Milky Way, single-dish radio beams typically cover size scales of tens to hundreds of GMC-sized diameters in nearby galaxies, and even interferometric beams correspond to size scales of a few GMCs. (A GMC has a typical diameter of 50 pc; Blitz 1987.) The disparate size scales over which these observations have been made preclude a fair comparison of these different regions. In this paper, we place ourselves at the telescope of an imaginary observer in a nearby galaxy, and we present a systematic study of molecular cloud properties in the Milky Way on size scales of GMCs and larger.

For the bulge of the Milky Way, we use the studies of Bally et al. (1987) (as presented in Helfer & Blitz 1993) and Jackson et al. (1996). We also present new observations of the disk of the Milky Way, which are divided into two types. First, we observed five local GMCs, one high-latitude cloud, and a distant outer-galaxy molecular cloud over their entire extents in CO, HCN and CS, in order to make the first measurements of dense gas ratios over a sample of whole clouds. Second, we surveyed some  $40^\circ$  in the first quadrant of the Milky Way using an unbiased sampling in order to determine the dense gas ratios in the Galactic plane, where the number density of molecular clouds is relatively high compared

with the local environment.

Throughout this study, we assume that the Sun lies at a distance of  $R_o = 8.5$  kpc from the Galactic Center.

## 2. Line Ratios as Tracers of High-Pressure Gas

In this study, we use as a qualitative measure of pressure the line ratios of the 3 mm transitions of HCN and CS to that of CO. Here, we examine the excitation characteristics of these molecules in order to justify the use of these ratios as indicators of gas pressure. Since much of this study as well as current extragalactic research emphasizes HCN observations over CS observations, we consider the excitation of the HCN molecule in the following discussion.

For CO, the  $J = 1$  state lies only 5.5 K above the ground rotational state, and for HCN, the difference is only 4.3 K; this means that even rather cold gas has the energy to populate the  $J = 1$  state for both molecules. Since the population of the upper rotational states is accomplished primarily by collisional excitations, then to first order, the  $H_2$  density plays a more important role than does the kinetic temperature in the excitation of these molecules. Furthermore, since the CO molecule has a relatively low dipole moment compared to HCN (0.1 debye for CO, 3.0 debye for HCN), it takes much higher densities to excite the HCN molecule: the critical excitation density of HCN is about  $10^3$  times higher than that of CO.

With this general picture in mind, we ran model calculations using a large velocity gradient (LVG) radiative transfer code (provided by L.G. Mundy) to examine the excitation properties of the  $J = 1 - 0$  transitions of the HCN and CO molecules. We assumed the relative abundances  $[HCN]/[CO] = 10^{-4}$  and  $[CO]/[H_2] = 8 \times 10^{-5}$  for these calculations and ran models for gas at kinetic temperature of 15 K and 70 K. The models assume a velocity gradient of  $1 \text{ km s}^{-1} \text{ pc}^{-1}$ . The results of the calculations are summarized in Figure 1. The top row shows the results for a total  $H_2$  column density  $N(H_2) = 1.3 \times 10^{21} \text{ cm}^{-2}$ , and the bottom row is for  $N(H_2) = 1.3 \times 10^{22} \text{ cm}^{-2}$ . As the left panels show, the CO  $J = 1$  state is already reasonably well populated at densities of  $n(H_2) = 10^2 \text{ cm}^{-3}$ , and there is little variation in the line strengths as a function of density. By contrast, the middle panels show that, for densities below  $\lesssim 10^{4-5} \text{ cm}^{-3}$ , the radiation temperatures for the HCN  $J = 1 - 0$  transition are small; the biggest increase in line temperature occurs over the density interval  $\sim 10^{3.5} \text{ cm}^{-3} - 10^6 \text{ cm}^{-3}$ .

The line ratios  $T_R(HCN)/T_R(CO)$  are shown in the right panels of Figure 1. These panels show the general trend that for low temperature gas as well as for high temperature

gas at densities  $\lesssim 10^6 \text{ cm}^{-3}$ , a higher line ratio  $T_{\text{R}}(\text{HCN})/T_{\text{R}}(\text{CO})$  implies a higher density gas. Thus for gas at the center of the Milky Way, where  $T_{\text{K}} \sim 70 \text{ K}$  and  $N(\text{H}_2) \sim 10^{22} \text{ cm}^{-2}$ , the measured HCN to CO line ratios of 0.05 – 0.2 (Jackson et al. 1996; see § 5) imply densities of  $10^4 - 10^{5.3} \text{ cm}^{-3}$ , whereas the ratios of  $\sim 0.02 - 0.03$  measured in the Milky Way disk (§ 4.3), where  $T_{\text{K}} \sim 15 \text{ K}$  and  $N(\text{H}_2) \sim 10^{22} \text{ cm}^{-2}$ , imply mean densities of  $\sim 10^{3.5} \text{ cm}^{-3}$ . In summary, although the exact results implied by the LVG analysis are dependent on an accurate knowledge of a number of variables, including the column densities, abundances, kinetic temperatures and velocity gradients – for which there is no independent measure in this study – the general consistency between the known conditions in the Milky Way and the ratios measured in the Milky Way bulge and disk lend credibility to the use of these line ratios as a qualitative measure of the pressure in galaxies.

### 3. Solar Neighborhood GMCs

The clouds surveyed are listed in Table 1. The five sources that form the core of this study are the S88, S140, S269, Orion B, and Rosette molecular clouds; these are GMCs that lie within 4 kpc of the Sun. The source MBM 32 is a high-latitude molecular cloud, rather than a GMC; its mass is much lower than that of a typical GMC ( $M_{\text{MBM32}} \sim 100 M_{\odot}$ , while GMCs are typically taken to be clouds with mass  $\gtrsim 10^4$  or  $10^5 M_{\odot}$ , Blitz 1993), and it is not self-gravitating (Magnani, Blitz, & Mundy 1985). The source OGC2 is an distant outer-galaxy molecular cloud; at a heliocentric kinematic distance of 21 kpc, this cloud lies beyond the optical disk of the Milky Way.

#### 3.1. FCRAO 14 m Observations

We observed the clouds S88, S140<sup>2</sup>, S269, Orion B, and MBM 32 using the Five Colleges Radio Astronomy Observatory (FCRAO) 14 m telescope in New Salem, MA in 1993 March 17-23, May 17-23, and October 22-27. We used the QUARRY multibeam receiver, which is an array receiver of  $3 \times 5$  Schottky diode mixers; this allowed for fast mapping of large fields with good sampling in a reasonable amount of time. At that time, the backends were 15 32-channel spectrometers with a resolution of 1 MHz; at 100 GHz, this corresponds to a velocity resolution of  $3.0 \text{ km s}^{-1}$  over a bandwidth of  $96 \text{ km s}^{-1}$ . Typical system temperatures were 700 – 1500 K at 115 GHz and 400 – 900 K at 88 GHz and 98 GHz. The FWHM of the individual QUARRY beams is about  $55''$  at 100 GHz; at a

---

<sup>2</sup>CO map kindly provided by M.H. Heyer

canonical cloud distance of 2 kpc, this corresponds to a linear resolution of about 0.5 pc.

The goal was to simulate an observation of each source with a telescope that has a beam large enough to cover the entire extent of the cloud as defined by the CO emission, typically  $r = 20$  pc. The general observing strategy was to cover the entire extent of the cloud with 30 to 60 second integrations at each position in each of the species CO J = 1-0 (115.27 GHz), CS J = 2-1 (97.98 GHz), and HCN J = 1-0 (88.63 GHz). For most of the clouds observed, we sampled at full beamwidth spacing. In the case of Orion B, we sampled about one quarter of the cloud area with sparser sampling. The resulting maps include some 2300 spectra in the case of S269, all the way up to 23000 spectra for S140.

Since the large data sets precluded a visual inspection of all the individual spectra, we reduced the spectra using automated routines. The data were transferred from the FCRAO SPA format into the AT&T Bell Laboratories package COMB for reduction. First, the spectra were scanned automatically for channels with absolute values that were outside a given tolerance. For a given spectrum, if there were two adjacent channels which were outside the tolerance, or if there were more than three isolated channels that were outside the tolerance, then the spectrum was rejected from the data set. Otherwise, any isolated bad channels were overwritten with the average of the two adjacent channels (or, if the bad channel was at the edge of the spectrum, the bad channel was replaced by the value of its neighboring channel). A linear baseline<sup>3</sup> was then fit to each spectrum from channels outside the velocity limits of the line emission. We made maps of integrated intensity using a “cone interpolation” smoothing scheme that weights each pixel by  $(1 - \frac{r}{r_i})$ , where  $r_i$  is the interpolation radius, typically chosen to be 1' (but chosen to be 9' for the case of Orion B). A visual inspection of the maps allowed us to go back and eliminate corrupt spectra that had been missed in the automated reduction.

The data cubes were then transferred to the MIRIAD package (Sault, Teuben, & Wright 1995) for further processing. We used channel maps of the CO data to determine the velocity extent of emission in the clouds, and we made maps of integrated intensity in CO by summing over those channels with detected emission. Maps of CS integrated intensity were made with the same velocity coverage as that of the CO. The HCN molecule has triplet fine-structure lines in its J = 1-0 transition; the limits of integration for the HCN integrated intensity maps were therefore extended by  $-7 \text{ km s}^{-1}$  and  $+5 \text{ km s}^{-1}$  to account for the fine structure lines<sup>4</sup>. Finally, we created a mask of the CO, HCN, and CS maps to

---

<sup>3</sup>In the case of the Orion B CS and the S269 HCN and CS data, there were low-amplitude standing waves apparent in the averaged spectra which required a fourth-order polynomial fit to the baseline to correct.

<sup>4</sup>In the case of the S269 HCN data, we did not use the full extent of the fine-structure velocity range in

ensure that only pixels that had been sampled in all of the three species were included in the subsequent analysis.

### 3.1.1. *The FCRAO Maps*

The FCRAO maps are presented in Figure 2 continued. The CO emission from S140, for example, is distributed over some 40 pc which defines the extent of the GMC; however, the peak of the emission is strongly concentrated at the well-studied starforming core ( $\alpha(1950) = 22^h17^m42^s, \delta(1950) = 63^\circ04'$ ). Figure 2 continued shows the dramatic contrast between the extended CO emission and the emission from HCN and CS, which at the sensitivity of these observations is confined to the central  $\sim 2$  pc around the S140 core; all the clouds show the paucity of dense condensations in GMCs and demonstrate how little of the volume of a GMC contains cores with the physical conditions required to produce HCN and CS lines of substantial strengths. What we wish to determine from these observations is whether there is low-level emission, perhaps not detected in a single spectrum, but detected in the average of hundreds or thousands of spectra whose positions are located throughout the GMC, that contributes positively to the total integrated emission of the cloud.

It is worthwhile pointing out once again the challenge of observing objects of different size scales with modern single-dish telescopes and interferometers. The  $1'$  beam size of the observations is shown in the upper right corner of the S140 CO image in Figure 2 continued. Although this beam size is tiny compared to the size of the region mapped, it is comparable to the *primary* beam size of modern interferometers! At the distance of a nearby galaxy, e.g.  $d = 5$  Mpc, the same beam size corresponds to a size scale of 1500 pc. Clearly, the task of making meaningful comparisons of these disparate objects is exacerbated by the gross differences in the linear resolutions of their observations.

### 3.1.2. *Further Processing of the FCRAO Data*

Since the GMCs we mapped are not circularly symmetric, we developed an automated routine to measure the total CO, HCN, and CS fluxes and their ratios as a function of a threshold of CO emission, rather than as a function of the physical distance from the cloud core. The threshold of CO emission was characterized by multiples of the uncertainty in the CO integrated intensity map (see below) as  $I_{\text{clip}} = 0,3,6,9\dots \times \sigma_{\text{CO}}$ . For each clipping level,

---

the limits of integration.

a CO map was generated from the original integrated intensity map by including only those pixels whose absolute value exceeded  $I_{\text{clip}}$ . This new CO map was then used as a template with which to select the corresponding pixels in the HCN and CS maps.

The results of this processing for S140, S88, Orion B, S269, and MBM32 are presented in Figure 3. The threshold levels of CO,  $I_{\text{clip}}$ , are represented as an effective radius  $r_{\text{eff}}$  in each cloud, where  $r_{\text{eff}} = 0.5\sqrt{Nd} \Delta x$ ;  $N$  is the number of pixels included in each map (where the clipping level was set by  $I_{\text{clip}}$ ),  $d$  is the distance to the cloud, and  $\Delta x$  is the angular extent of an individual pixel. The analysis may thus be thought of as a kind of “aperture photometry” so that Figure 3 represents the summed intensities of CO, HCN, and CS as a function of the effective radius of the aperture. We note that near the core of each cloud, the effective radius is the same as the physical radius; the physical and effective radii diverge at distances of a few parsecs.

In Figure 3, the summed CO intensity  $\Sigma I(\text{CO})$  rises monotonically as a function of the effective radius for each the clouds observed. This is easily understood, since the cloud is defined by its CO extent and more and more of the cloud is included in the sum as the effective radius increases. For the HCN and CS emission, we expect that the summed intensities should also rise monotonically, but that at some  $r_{\text{eff}}$  they might reach some plateau that represents the total emission in HCN or CS. As Figure 3 shows, this is the case for e.g. the S140 HCN panel and the S88 panels. But Figure 3 also shows that the total intensity *decreases* for some of the clouds at  $r_{\text{eff}} \gtrsim 5$  pc, e.g. for S140 CS and for Orion B HCN and CS. These decreases are not physical; they are representative of systematic errors that appear at the highest sensitivities in the maps (see below). Figure 3 also shows that low-level emission from HCN and CS generally contributes positively to the summed intensities at least out to effective radii of  $\sim 5$  pc.

The ratios  $I_{\text{HCN}}/I_{\text{CO}}$  and  $I_{\text{CS}}/I_{\text{CO}}$  are shown as a function of the effective radius of the aperture in Figure 4. As this figure shows, the ratios are strong functions of the effective radius  $r_{\text{eff}}$ . The peak values for  $I_{\text{HCN}}/I_{\text{CO}}$  range from 0.1 – 0.3 for all four clouds on size scales of  $r_{\text{eff}} \leq 1$  pc, but by  $r_{\text{eff}} = 5$  pc,  $I_{\text{HCN}}/I_{\text{CO}}$  has dropped to 0.04 or below, and by  $r_{\text{eff}} \geq 10$  pc,  $I_{\text{HCN}}/I_{\text{CO}}$  is  $\leq 0.02$  for all four clouds. The ratio  $I_{\text{CS}}/I_{\text{CO}}$  shows a similar trend.

The average ratios over the entire clouds are  $\langle I_{\text{HCN}} \rangle / \langle I_{\text{CO}} \rangle = 0.007 - 0.019$  and  $\langle I_{\text{CS}} \rangle / \langle I_{\text{CO}} \rangle = 0.006 - 0.020$ . For MBM 32, neither HCN nor CS was detected; the  $3\sigma$  upper limits were  $< 0.015$  for  $\langle I_{\text{HCN}} \rangle / \langle I_{\text{CO}} \rangle$  and  $< 0.009$  for  $\langle I_{\text{CS}} \rangle / \langle I_{\text{CO}} \rangle$ .

### 3.1.3. *Limitations of the Observations*

The experiment that we have described above, i.e. that of making high sensitivity measurements of low-level emission, is a particularly challenging one to do with good accuracy at millimeter wavelengths. At high sensitivities, systematic uncertainties dominate the random errors and one must pay special attention to problems like low-amplitude standing waves in the telescope spectrometer (see footnote 4 in § 3.1) and the details of the baseline fitting. In these QUARRY observations, the spectrometer we used had only 32 channels per beam, and since the velocities with potential emission were excluded from the baseline fits, the fits typically relied on data from 22 to 25 channels only. Given the small number of channels available, we restricted the baseline fits to linear functions wherever possible. In addition to the possibility of low-amplitude standing waves across the bandpass of the observations, there were also instances of individual channels that appeared to be systematically high or low, again at a level that was subtle enough not to be detected in an individual spectrum. We note that the errors shown in Figure 4 are the statistical errors only. The systematic errors are much larger; we estimate that they are at least comparable to and probably somewhat larger than the magnitude of the ratios for radii with  $r_{\text{eff}} \gtrsim 5$  pc. We conclude that the uncertainties in the average ratios measured over the five clouds measured at FCRAO are probably  $\pm 0.02$  or higher.

## 3.2. NRAO 12 m Observations

The OGC2 and Rosette clouds were observed with the NRAO 12 m telescope on Kitt Peak, AZ in 1993 June 15-20. Typical system temperatures were 350 – 800 K at 115 GHz and 150 – 400 K at 89 GHz and 98 GHz. For the Rosette observations, the spectrometer was two  $128 \times 250$  kHz filter banks which we used to measure orthogonal polarizations; we used two  $128 \times 100$  kHz filter banks for the OGC2 cloud. At 100 GHz, the telescope half-power beam width is  $63''$ . We mapped each cloud in CO, HCN, and CS and tried to cover the entire area of each cloud; for the Rosette cloud, this meant using a somewhat sparse sampling with a pointing spacing of  $12'$ . For the OGC2 cloud, we sampled at  $1'$  spacing.

We removed linear baselines from the emission-free regions of the spectra using the AT&T Bell Labs package COMB. For both clouds, we did not detect HCN or CS emission within the sensitivity of our observations. In the case of the Rosette, Blitz & Stark (1992, private communication) and Williams (1995) detected CS emission towards several clumps; it is likely that we missed these clumps because of our sparse sampling. The  $3\sigma$  upper limits to the ratios for these clouds are  $I_{\text{HCN}}/I_{\text{CO}} \leq 0.013$  and  $I_{\text{CS}}/I_{\text{CO}} \leq 0.011$  for the Rosette and

$I_{\text{HCN}}/I_{\text{CO}} \leq .016$  and  $I_{\text{CS}}/I_{\text{CO}} \leq 0.013$  for OGC2. The  $3\sigma$  upper limit for the Rosette ratio  $I_{\text{CS}}/I_{\text{CO}}$  is in good agreement with the ratio calculated in Appendix B of Helfer & Blitz (1993),  $I_{\text{CS}}/I_{\text{CO}} = 0.010$ .

### 3.3. Results of Cloud Study

The cloud ratios for the FCRAO and NRAO studies are summarized in Table 2<sup>5</sup>. If we take the  $3\sigma$  upper limits as the measured ratios for the Rosette nondetections, then the average ratios over the five GMCs measured are  $\langle I_{\text{HCN}}/I_{\text{CO}} \rangle = 0.014 \pm 0.02$  and  $\langle I_{\text{CS}}/I_{\text{CO}} \rangle = 0.013 \pm 0.02$ .<sup>6</sup> These numbers are representative of the average ratios over individual GMCs on size scales of  $\sim 40$  pc diameter. From Figure 4, it is clear that the star-forming cores that occur on size scales of  $\lesssim 1$  pc in GMCs are characterized by much higher ratios than is typical for most of the area of the GMC. This disparity is naturally explained by the difference in the gas density between the cores and the ambient gas across the extent of a GMC.

In cloud cores, the HCN emission usually dominates that of CS on scales of a few pc or smaller (see Figure 4). This is also seen on all size scales ( $\sim 1$  pc - 3 kpc) in the Milky Way plane (see Figures 8 and 9) as well as over hundreds of pc in the centers of galaxies (Helfer & Blitz 1993; § 5). Over the entire GMCs, however, the ratios  $I_{\text{HCN}}/I_{\text{CO}}$  and  $I_{\text{CS}}/I_{\text{CO}}$  are the same to within their measurement errors. Since the ratios over the entire GMCs are dominated by their uncertainties, it is not clear if this effect is a physical one or an artifact of the measurements.

## 4. Milky Way Plane Survey

### 4.1. Observations

We observed HCN, CS, and CO using an unbiased sampling in the first quadrant of the plane of the Milky Way using the NRAO 12 m telescope in 1993 June 15 – 20. We made position-switched observations using reference positions from Waller & Tacconi-Garman

---

<sup>5</sup>For the FCRAO data, we used the peaks of the summed HCN and CS intensities in Figure 3 to compute the ratios.

<sup>6</sup>Given the systematic problems with the FCRAO data, we assign both averages an uncertainty of  $\pm 0.02$ , rather than the uncertainty in the mean  $\sigma/N^{0.5}$ .

(1992). The system temperatures ranged from 300 – 600 K at 115 GHz to 165 – 500 K at 89 GHz and 98 GHz. We observed orthogonal polarizations and averaged the spectra from the two channels. The backend was a hybrid spectrometer which was configured to achieve 0.39 MHz (1.2 km s<sup>-1</sup> at 100 GHz) resolution over a 300 MHz (900 km s<sup>-1</sup> at 100 GHz) bandwidth or 0.78 MHz resolution over a 600 MHz bandwidth. Typical integrations were 2 minutes on each position for the CO observations and 6 minutes for the HCN and CS, though we were able to integrate longer on selected individual positions in HCN and CS. The data were processed using the AT&T Bell Laboratories package COMB. Since there were standing waves in the 300 and 600 MHz bandpass, we fit polynomial functions to the baselines excluding channels in the velocity range where there was possible emission (-30 – 140 km s<sup>-1</sup>). As a check to the fits, we also calculated a linear or quadratic fit to the baseline using emission-free channels over a limited range of the bandpass (-100 – 250 km s<sup>-1</sup>); the results were comparable to the higher-order fits.

The survey coverage included positions in the Milky Way plane ( $b = 0^\circ$ ) at longitudes  $15.^\circ5 \leq l \leq 55.^\circ5$  in steps of  $\Delta l = 1^\circ$ . Some of the spectra were rejected because of excessive standing wave problems or other corruptions; in all, there were 41 positions which were successfully observed in CO, 37 positions in HCN, and 31 positions in CS. There were 30 longitudes which were observed in all three species. We use these 30 positions in the following analysis; their spectra are shown in Figure 5.

## 4.2. Geometric Considerations and Basic Results of Plane Survey

For any given line of sight  $l$ , an observed velocity  $v_{\text{obs}}$  corresponds to a unique Galactocentric distance  $R$  via the geometric relationship  $v_{\text{obs}} = V R/R_o \sin l - V_o \sin l$ , where  $V$  and  $V_o$  represent the circular velocities at distances  $R$  and  $R_o$ . The validity of this relationship breaks down for small longitudes  $l$ , since large noncircular motions dominate in the region of the Galactic Center. We have avoided this complication by restricting our observations to  $l > 15^\circ$ . The relationship is also invalid for  $|v_{\text{obs}}| \leq 20 \text{ km s}^{-1}$  since the random motions of nearby clouds may dominate their projected circular motions.

We can illustrate some basic results of the plane survey by examining the CO, HCN, and CS spectra at a sample longitude,  $l = 30.5^\circ$  (Figure 6). The CO spectrum at this longitude shows peaks at many different velocities, which correspond to clouds at different distances<sup>7</sup> along the line of sight. The strongest features in the CO spectrum, those at 40

---

<sup>7</sup>Throughout this study, we calculate kinematic distances assuming a flat rotation curve with  $V_o = 220 \text{ km s}^{-1}$  and  $R_o = 8.5 \text{ kpc}$ .

km s<sup>-1</sup>, 90 km s<sup>-1</sup>, and 110 km s<sup>-1</sup>, show corresponding emission in HCN and CS. These features are emitted from gas at kinematic distances from the Galactic Center of 6.3 kpc, 4.7 kpc, and 4.3 kpc. The feature at R = 6.3 kpc could be at a heliocentric distance of 11.9 kpc or 2.7 kpc; at these distances, the 1' resolution of the observations corresponds to a linear resolution of 3.5 pc or 0.79 pc. In general, the characteristic linear resolution of the plane survey is  $\sim 1$  pc; this is much smaller than the size scale of a typical GMC ( $\sim 40$  pc, see Figure 2 continued), so a feature may be considered a “pencil-beam” observation through some random location in a GMC.

There are several points worth noting about the comparison of HCN and CS features to the CO emission in Figure 6: (1) The linewidths of the features are the same (allowing for the triplet fine structure of the HCN line, which causes a broadening of  $\Delta v_{-7}^{+5}$  km s<sup>-1</sup>). (2) The shapes of the features are quite similar. Both these points emphasize the fact that the CO, the HCN and the CS emission at a given velocity all trace gas at the same physical region. (3) The strengths of the HCN and CS emission vary with respect to the CO emission from one feature to another; this suggests that the excitation conditions or abundances vary among the different positions.

### 4.3. The Radial Distribution of Dense Gas Emission in the Plane

In order to determine the dense gas distribution as a function of radius in the plane of the Milky Way, we binned the inner Galaxy in concentric annuli of width  $\Delta R = 200$  pc and used the CO, HCN, and CS spectra to calculate the emissivities  $J_l = 1/\Delta L \int T_R^* dv$ , where the velocity limits of integration were determined for each bin from the relationship  $v_{\text{obs}} = V R/R_o \sin l - V_o \sin l$ . The emissivity represents the integrated intensity normalized by the path length  $\Delta L$  through an annulus along the line of sight to the Sun. The data from all 30 longitudes were then combined to form an average  $\langle J \rangle(R) = 1/30 \sum_l J_l(R)$  for each of the three molecules.

Figure 7 shows the radial distributions of CO, HCN, and CS emissivities. The CO distribution agrees well with surveys of the Milky Way that include much more complete sampling (e.g. Sanders, Solomon, & Scoville 1984; Dame et al. 1987). In particular, there is a relative maximum of CO emission at radii in the range  $4 < R < 5.5$  kpc that falls off with R at larger radii. The emissivities from HCN and CS show similar distributions to that of the CO, with an enhancement of emission at the position of the relative maximum.

The ratios of emission are shown in Figure 8. There is a moderate tendency for higher  $\langle J \rangle(\text{HCN})/\langle J \rangle(\text{CO})$  and  $\langle J \rangle(\text{CS})/\langle J \rangle(\text{CO})$  towards inner Galactocentric radii; linear

fits to the data yield  $\langle J \rangle(\text{HCN})/\langle J \rangle(\text{CO}) = 0.049 - 0.005 R$  and  $\langle J \rangle(\text{CS})/\langle J \rangle(\text{CO}) = 0.040 - 0.005 R$ . The upturn in  $\langle J \rangle(\text{HCN})/\langle J \rangle(\text{CO})$  at  $R \gtrsim 6.6$  kpc suggests that local excitation effects might have an important effect at a level of  $\pm 0.01$  in the ratios; alternatively, since the sensitivity of the survey is poorest at the endpoints, the values of the ratios may be artificially high at these positions. If the radial trend is real, we note that it is modest in comparison with the typical measurement uncertainties. The data are reasonably well represented by their average values (computed over ratios with  $> 2\sigma$  detections),  $\langle J \rangle(\text{HCN})/\langle J \rangle(\text{CO}) = 0.026 \pm 0.008$  and  $\langle J \rangle(\text{CS})/\langle J \rangle(\text{CO}) = 0.018 \pm 0.008$  over the region  $3.5 < R < 7$  kpc.

The radial distribution of molecular cloud properties has also been studied by Liszt, Burton, & Xiang (1984), Liszt (1993), Sanders et al. (1993), Handa et al. (1993), Liszt (1995), and Sakamoto et al. (1995, 1996); the results of these studies are contradictory. Liszt et al. (1984) studied the variation of the  $^{12}\text{CO}/^{13}\text{CO}$  J=1–0 emission line ratio in the first quadrant of the Galactic disk and found a tendency for lower  $^{12}\text{CO}/^{13}\text{CO}$  ratios towards inner Galactocentric radii; they interpreted this result as evidence for higher mean hydrogen column densities at inner radii. However, Liszt (1993) studied the J=2–1 to J=1–0 emission ratio of  $^{13}\text{CO}$  in the same region and found no systematic variation across the Galactic disk; he therefore concluded that the mean densities do not vary as a function of radius and that abundance effects probably cause the variation in the  $^{12}\text{CO}/^{13}\text{CO}$  ratios. Liszt’s (1995) survey of  $\text{HCO}^+$  in the first quadrant shows a moderate tendency towards higher  $\text{HCO}^+ / ^{13}\text{CO}$  ratios at inner radii, which he also interprets as abundance effects. In contrast to Liszt’s J=2–1 to J=1–0  $^{13}\text{CO}$  study, Handa et al. (1993) and Sakamoto et al. (1995, 1996) presented an extensive J=2–1  $^{12}\text{CO}$  survey of the first quadrant, compared their data to the J=1–0  $^{12}\text{CO}$  Columbia survey, and found a systematic gradient across the disk; these authors concluded that the gas in the inner galaxy is on average warmer and more dense than that in the solar neighborhood. Finally, Sanders et al. (1993) used the J=3–2, J=2–1, and J=1–0 transitions of both  $^{12}\text{CO}$  and  $^{13}\text{CO}$  and found no gradient across the disk in any of the line ratios. These contradictory studies as well as the work presented here all show that if there is a trend in the physical properties of disk clouds as a function of radius interior to the Solar circle, then it is a modest one.

There is no clear radial trend in the ratio of HCN to CS emissivity. On average, the HCN emissivity is stronger than the CS emissivity by a factor of  $\sim 2$ . This is similar to what is observed in the centers of other galaxies (Helfer & Blitz 1993) and in the Milky Way (see below).

#### 4.4. Moderate Densities in the Plane “Features”

In nearby GMCs, less than 5% of the area of a cloud has detectable emission from HCN or CS at the sensitivity achievable in an integration time of a few minutes (this study, see Figure 2 continued). The typical dense gas ratios over these pc-scale cores are  $I_{\text{HCN}}/I_{\text{CO}} \gtrsim 0.1$ . We have seen that the ratios in the Milky Way plane are much lower than this, or  $I_{\text{HCN}}/I_{\text{CO}} = 0.026$  on average over size scales of 200 pc. We may now ask how the average ratios in the plane discussed in the previous section compare with the ratios over individual, pc-scale “features” in the plane spectra of Figure 5. To do this, we defined a “feature” by eye from an inspection of the CO spectra at each longitude: a “feature” was taken to be either an isolated spectral line or, where the line blending was too severe to choose a unique peak, the collection of emission that made up the blended line. Using limits of integration that covered the CO emission, we recorded the integrated intensity of CO and then measured the HCN and CS emission over the corresponding velocities. The ratios over these individual features are shown in Figure 9.

Although there is considerable spread in the ratios, on average the values are low, with the bulk of the ratios  $I_{\text{HCN}}/I_{\text{CO}}$  and  $I_{\text{CS}}/I_{\text{CO}}$  between 0.01 – 0.05. These ratios are consistent with the average ratios measured in the plane, rather than the ratios measured in the dense cores in GMCs (0.1 – 0.3); this suggests that the plane features are for the most part *not* dense cores that happen to intersect our line of sight, but rather that the emission is from gas of moderate density. This conclusion is supported by the low strengths of the HCN and CS lines in the plane: although the kinetic temperature of the gas is on the order of  $T_{\text{K}} = 10 - 15$  K (these temperatures are consistent with the observed peak CO line strengths of  $T_{\text{r}} = 5 - 10$  K), the antenna temperatures of the HCN and CS emission are typically 0.2 K or below (Figure 5). As the LVG modeling in § 2 suggests (see the lower middle panel of Figure 1, which shows  $T_{\text{r}}(\text{HCN})$  as a function of density for  $T_{\text{K}} = 15$  K and  $N(\text{H}_2) \sim 10^{22}$   $\text{cm}^{-2}$ ), the densities of the plane features are probably only a few times  $10^3$   $\text{cm}^{-3}$ .

Liszt (1995) recently presented an unbiased survey of the 3 mm emission from  $\text{HCO}^+$  (as well as selected positions in HCN, CS, and  $\text{C}_2\text{H}$ ) in the Milky Way plane and reached a similar conclusion, namely, that the ubiquity and low intensities of the emission from these species imply that the gas is at moderate densities.

## 5. The Distribution of Dense Gas Ratios in the Milky Way

To complete our synthesis of dense gas observations in the Milky Way, we turn now to the center of the Galaxy, which was observed in CS by Bally et al. (1987) and in HCN

by Jackson et al. (1996). In this region, CS and HCN emission are distributed throughout the inner  $d \sim 500$  pc ( $-1^\circ \leq l \leq 1.^\circ 8$ ), which is characterized by the highest molecular emissivity in the Galaxy (the surface density of CO is about 60 times higher in the bulge than the average at the Solar circle, Sanders et al. 1984). The dense gas emission extends some 12 pc ( $0.08^\circ$ ) out of the plane of the Milky Way (Jackson et al. 1996). Averaged over the central 500 pc, the CS to CO ratio is  $I_{\text{CS}}/I_{\text{CO}} = 0.027 \pm 0.006$  (Helfer & Blitz 1993). The HCN to CO ratio ranges from 0.04 to about 0.12 on small scales within the bulge region; averaged over the central 600 pc, the ratio is  $I_{\text{HCN}}/I_{\text{CO}} = 0.081^8 \pm 0.004$ . We note that the errors quoted here are formal uncertainties; these may underestimate the uncertainties due to absolute calibration errors.

Armed with the HCN and CS studies of the Galactic Center (Bally et al. 1987; Helfer & Blitz 1993; Jackson et al. 1996), the plane of the Milky Way (§ 4), and clouds near the Sun (§ 3), we now wish to compare the distribution of the ratios of dense gas as a function of location in the Milky Way. These ratios are summarized in Figure 10. Clearly, there is a radial trend in the ratios: they are higher by a factor of 3 in  $I_{\text{HCN}}/I_{\text{CO}}$  and 1.5 in  $I_{\text{CS}}/I_{\text{CO}}$  in the center of the Milky Way when compared with the average ratios in the disk. Although the plane  $I_{\text{HCN}}/I_{\text{CO}}$  ratio is about 0.01 higher than that measured over nearby GMCs (the  $I_{\text{CS}}/I_{\text{CO}}$  differs by even less), the differences are within the measurement uncertainties. We therefore conclude that, while there might be a modest trend towards higher ratios for smaller radii for  $R > 3$  kpc, by far the dominant result is the contrast between the high ratios in the Milky Way bulge and the lower ratios in the disk. The high ratios in the bulge are most likely caused by a combination of higher gas densities as well as higher kinetic temperatures in the bulge gas:  $n(\text{H}_2) \sim 10^4 \text{ cm}^{-3}$  and  $T_{\text{K}} \sim 70$  K in the bulge, while  $n(\text{H}_2) \sim 10^{2.5-3} \text{ cm}^{-3}$  and  $T_{\text{K}} \sim 15$  K in the disk (Güsten 1989 and references therein). The correlation between the dense gas ratios and the known properties of molecular gas in the bulge and disk of the Milky Way gives credibility to the use of dense gas to CO emission ratios as a tracer of different physical properties in galaxies.

---

<sup>8</sup> Jackson et al. 1996. We use their correction for HCN and CO emission at nonzero Galactic latitude. In their “aperture photometry”, Jackson et al. smooth their HCN map to a spatial resolution larger than that of their CO map by a factor of  $\lambda(\text{HCN})/\lambda(\text{CO})$  in order to emulate the single-dish measurements of extragalactic ratios. This correction is not appropriate for comparison with this study; we therefore “re-correct” their ratio so that it is appropriate for direct comparison to these results.

## 6. The Relation Between Dense Gas Ratios and Pressure

Any diffuse gaseous component in the Milky Way has a total internal pressure that is at least as high as that determined by the condition of hydrostatic equilibrium with the stellar gravitational potential. The total gas pressure may be represented as  $P_g = 2\pi G\rho_*\Sigma_g h_g$ , where  $\rho_*$  is the stellar density,  $\Sigma_g$  is the total gas surface density, and  $h_g$  is the scale height of the gas (Spergel & Blitz 1992). Using this expression for the total gas pressure, we calculated the pressure at the positions of five points for which we have measured values for the ratio  $I_{\text{HCN}}/I_{\text{CO}}$ : the Galactic Center, three positions in the Milky Way plane (using binned data from Figure 8), and the average ratio over individual GMCs. For  $\rho_*$ , we assumed an exponential distribution as a function of radius, with a scale length of 3 kpc (Spergel, Malhotra, & Blitz 1996); to set the scale for  $\rho_*$ , we used the local value at the solar circle of  $0.1 M_\odot \text{pc}^{-3}$  (Gould 1995). We used the CO and HI surface densities compiled by Dame (1993). The CO scale heights  $h_g$  are from Sanders et al. (1984) and Dame et al. (1987). At the Galactic Center, we used  $\rho_* = 25 M_\odot \text{pc}^{-3}$  (Spergel & Blitz 1992) and  $\Sigma_g(\text{CO}) = 180 M_\odot \text{pc}^{-2}$  (based on Sanders et al. 1984).

The results of this calculation are shown in Figure 11. Each point is labeled with its distance from the Galactic Center, so the progression in both pressure and in  $I_{\text{HCN}}/I_{\text{CO}}$  is correlated with distance. A fit to the data yields the result that the ratios  $I_{\text{HCN}}/I_{\text{CO}}$  rise with pressure as  $I_{\text{HCN}}/I_{\text{CO}} \propto P^{0.19 \pm 0.04}$ . In § 2, the claim was made that the ratio of emissions  $I_{\text{HCN}}/I_{\text{CO}}$  could be used as a qualitative indicator of pressure in a galaxy. Figure 11 suggests that the ratio  $I_{\text{HCN}}/I_{\text{CO}}$  may be a reasonable *quantitative* measure of pressure. It remains a topic of future research to determine whether this relation holds in external galaxies, and if so, whether the slope of the correlation is a universal one.

## 7. Conclusions

We have presented a systematic examination of the 3 mm emission from HCN, CS, and CO on size scales of GMCs ( $\sim 40$  pc) and larger in the bulge and disk of the Milky Way. This study combined new observations of individual GMCs and the Milky Way plane with published studies of the inner 500 pc of the Galaxy.

### 7.1. Results from the GMC survey

We surveyed five molecular clouds with the FCRAO 14 m telescope using the QUARRY multibeam receiver and an additional two clouds using the NRAO 12 m telescope. As seen

in the FCRAO maps, less than 5% of the area of a cloud has detectable emission from HCN or CS at the sensitivity achievable in an integration time of a few minutes. The ratios  $I_{\text{HCN}}/I_{\text{CO}}$  and  $I_{\text{CS}}/I_{\text{CO}}$  are strong functions of the effective radius of the clouds: the peak values for  $I_{\text{HCN}}/I_{\text{CO}}$  range from 0.1 – 0.3 over size scales of  $\leq 1$  pc, but by  $r_{\text{eff}} = 5$  pc,  $I_{\text{HCN}}/I_{\text{CO}}$  drops to 0.04 or below, and by  $r_{\text{eff}} \geq 10$  pc,  $I_{\text{HCN}}/I_{\text{CO}}$  is  $< .02$ . Similar trends are seen for  $I_{\text{CS}}/I_{\text{CO}}$ . Taking into account the systematic uncertainties in the data, the average ratios over the GMCs measured are  $\langle I_{\text{HCN}}/I_{\text{CO}} \rangle = 0.014 \pm 0.02$  and  $\langle I_{\text{CS}}/I_{\text{CO}} \rangle = 0.013 \pm 0.02$ . These numbers represent the average ratios over individual GMCs near the Sun on size scales of  $\sim 40$  pc diameter. The disparity between the higher ratios in the pc-sized cloud cores and the low ratios characteristic of entire GMCs is naturally explained by the difference in gas density between the cores and the ambient gas across the full extent of a GMC.

## 7.2. Results from the Milky Way Plane Survey

We surveyed HCN, CS, and CO using an unbiased sampling over some 40° of the first quadrant of the plane of the Milky Way using the NRAO 12 m telescope. Features from HCN and CS were surprisingly common. When compared to the corresponding CO emission, the HCN and CS features showed the same linewidths and line shapes, which implies that the CO, HCN, and CS emission at a given velocity all trace gas from the same physical region. However, the relative strengths of the lines vary from one feature to another; this suggests that the excitation conditions or abundances vary among the different positions.

On average, the ratios  $I_{\text{HCN}}/I_{\text{CO}}$  and  $I_{\text{CS}}/I_{\text{CO}}$  range between 0.01 – 0.05 over individual, pc-sized features in the plane survey. These ratios are much lower than those measured in the cores of GMCs (0.1 – 0.3); this suggests that the features are for the most part *not* dense cores that happen to intersect our line of sight, but rather that the gas is at moderate density. This conclusion is supported by the relatively weak strengths of the emission lines seen in HCN and CS. These results were also noted in the  $\text{HCO}^+$  survey of the Milky Way plane by Liszt (1995).

We binned the plane data as a function of Galactocentric radius in concentric annuli of width 200 pc and computed the average  $I_{\text{HCN}}/I_{\text{CO}}$  and  $I_{\text{CS}}/I_{\text{CO}}$  for the different bins. There is a moderate tendency for higher ratios towards inner Galactocentric radii; however, the data are well represented by their averages:  $I_{\text{HCN}}/I_{\text{CO}} = 0.026 \pm 0.008$  and  $I_{\text{CS}}/I_{\text{CO}} = 0.018 \pm 0.008$  over the region  $3.5 < R < 7$  kpc.

### 7.3. General Results

We find a strong trend in the ratios of HCN and CS emission as a function of location in the Milky Way: in the bulge,  $I_{\text{HCN}}/I_{\text{CO}} = 0.081 \pm 0.004$ , in the plane,  $I_{\text{HCN}}/I_{\text{CO}} = 0.026 \pm 0.008$  on average, and over the full extent of nearby GMCs,  $I_{\text{HCN}}/I_{\text{CO}} = 0.014 \pm 0.02$ . Similar trends are seen for CS: in the bulge,  $I_{\text{CS}}/I_{\text{CO}} = 0.027 \pm 0.006$ , in the plane,  $I_{\text{CS}}/I_{\text{CO}} = 0.018 \pm 0.008$  on average, and over the full extent of nearby GMCs,  $I_{\text{CS}}/I_{\text{CO}} = 0.013 \pm 0.02$ . (Formal uncertainties are quoted; these may underestimate the uncertainties due to absolute calibration errors.)

The dominant result of this study is the contrast between the high ratios in the Milky Way bulge and the lower ratios in the disk. The high bulge ratios are likely caused by a combination of higher gas densities and higher kinetic temperatures in the bulge gas (Güsten 1989). The correlation between the HCN and CS emission ratios and the known properties of molecular gas in the bulge and disk of the Milky Way gives credibility to the use of dense gas to CO emission ratios as a tracer of different physical properties in galaxies.

Using stellar and gas surface densities from the literature, we calculated the total gas pressure as a function of radius in the Milky Way and compared the results with the  $I_{\text{HCN}}/I_{\text{CO}}$  ratios we measured. A fit to the data shows that the ratios  $I_{\text{HCN}}/I_{\text{CO}}$  rise with pressure as  $I_{\text{HCN}}/I_{\text{CO}} \propto P^{0.19 \pm 0.04}$ . In this paper, we have claimed that  $I_{\text{HCN}}/I_{\text{CO}}$  could be used as a qualitative indicator of pressure in a galaxy; this result suggests that  $I_{\text{HCN}}/I_{\text{CO}}$  may be a reasonable quantitative measure of pressure.

We thank the referee, Jim Jackson, for useful comments on the manuscript. We thank Mark Heyer for his advice with the FCRAO observations and for supplying us with with CO map of S140; thanks also to the FCRAO staff for making the cloud observations possible. We thank the staff at NRAO for their assistance with the plane and cloud observations. TTH thanks Jack Welch for his hospitality while visiting UC Berkeley, and she thanks John Lugten for many discussions about the details of the data analysis and the resulting science. This research was supported by grants from the National Science Foundation and the State of Maryland.

## REFERENCES

- Bally, J., Stark, A.A., Wilson, R.W., & Henkel, C. 1987, *ApJS*, 65, 13
- Blitz, L. 1987, in *Physical Processes in Interstellar Clouds*, ed. G.E. Morfill & M. Scholer (Dordrecht:Reidel), 35
- Blitz, L. 1993, in *Protostars and Planets III*, ed. E.H. Levy & J.I. Lunine (Tucson:Univ. of Arizona Press), 12
- Dame, T.M. 1993, in *Back to the Galaxy*, eds. S.S. Holt & F. Verter (New York:AIP), AIP Conference Proceedings 278, 267
- Dame, T.M., Ungerechts, H., Cohen, R.S., de Geus, E.J., Grenier, I.A., May, J., Murphy, D.C., Nyman, L.-Å., & Thaddeus, P. 1987, *ApJ*, 322, 706
- Digel, S., de Geus, E., & Thaddeus, P. 1994, *ApJ*, 422, 92
- Gould, A. 1996, in *Unsolved Problems of the Milky Way*, eds. L. Blitz & P. Teuben (Dordrecht:Kluwer), 651
- Güsten, R. 1989, in *The Center of the Galaxy*, ed. Morris, M. (Dordrecht:Kluwer), 89
- Handa, T., Hasegawa, T., Hayashi, M., Sakamoto, S., Oka, T., & Dame, T.M. 1993, in *Back to the Galaxy*, eds. S.S. Holt & F. Verter (New York:AIP), AIP Conference Proceedings 278, 315
- Helfer, T.T. & Blitz, L. 1993, *ApJ*, 419, 86
- Jackson, J.M., Heyer, M.H., Paglione, T.A.D., & Bolatto, A.D. 1996, *ApJ*, 456, 91
- Lada, E.A., Bally, J., & Stark, A.A. 1991, *ApJ*, 368, 432
- Liszt, H.S. 1993, *ApJ*, 411, 720
- Liszt, H.S. 1995, *ApJ*, 442, 163
- Liszt, H.S., Burton, W.B., & Xiang, D.L. 1984, *A&A*, 140, 303
- Magnani, L., Blitz, L., & Mundy, L.G. 1985, *ApJ*, 295, 402
- Nguyen-Q-Rieu, Jackson, J. M., Henkel, C., Truong-Bach, & Mauersberger, R. 1992, *ApJ*, 399, 521
- Sakamoto, S., Hasegawa, T., Hayashi, M., Handa, T., & Oka, T. 1995, *ApJS*, 100, 125

———. 1996, submitted to ApJ

Sanders, D.B., Scoville, N.Z., Tilanus, R.P.J., Wang, Z., & Zhou, S. 1993, in *Back to the Galaxy*, eds. S.S. Holt & F. Verter (New York:AIP), AIP Conference Proceedings 278, 311

Sanders, D.B., Solomon, P.M., & Scoville, N.Z. 1984, ApJ, 276, 182

Sault, R.J., Teuben, P.J., & Wright, M.C.H. 1995, in *Astronomical Data Analysis Software and Systems IV*, eds. R.A. Shaw, H.E. Payne, & J.J.E. Hayes, A.S.P. Conference Series 77, 433

Spergel, D.N. & Blitz, L. 1992, Nature, 357, 665

Spergel, D.N., Malhotra, S., & Blitz, L. 1996, in *Spiral Galaxies in the Near Infrared*, eds. D. Minnitti & H.-W. Rix, in press

Waller, W.H. & Tacconi-Garman, L.E. 1992, ApJS, 80 305

Williams, J.P. 1995, Ph.D. thesis, University of California

Table 1. Cloud Sources

Cloud	$l$ ( $^{\circ}$ )	$b$ ( $^{\circ}$ )	$d$ (kpc)	R (kpc)	$v_{\text{LSR}}^{\text{a}}$ ( $\text{km s}^{-1}$ )
S88	61.47	0.10	2.0	7.8	21
S140	106.76	5.28	0.9	8.8	-8
S269	196.45	-1.68	3.8	12.2	17.5
Orion B	206.53	-16.35	0.4	8.6	10
Rosette	206.86	-2.21	1.6	10.0	16
OGC2 <sup>b</sup>	137.75	-1.00	21	28	-103
MBM 32 <sup>c</sup>	147.20	40.67	0.1	8.6	0

<sup>a</sup>  $v_{\text{LSR}}$  is defined by the radio convention,  $v_{\text{LSR}}/c = \Delta\lambda/\lambda_o$ , where  $\lambda_o$  is the wavelength in the rest frame of the source.

<sup>b</sup> Outer Galaxy Cloud 2, from Digel, de Geus, & Thaddeus 1994.

<sup>c</sup> High-latitude cloud from Magnani, Blitz, & Mundy 1985.

Table 2. Results from Cloud Surveys

Cloud	$I_{\text{HCN}}/I_{\text{CO}}$	$I_{\text{CS}}/I_{\text{CO}}$	Telescope
S88	0.016 <sup>a</sup>	0.013	FCRAO
S140	0.019	0.013	FCRAO
S269	0.007 <sup>b</sup>	0.020	FCRAO
Orion B	0.014	0.006 <sup>b,c</sup>	FCRAO
Rosette	$\leq 0.013^{\text{d}}$	$\leq 0.011^{\text{c}}$	NRAO
OGC2	$\leq 0.016$	$\leq 0.013$	NRAO
MBM 32	$\leq 0.015$	$\leq 0.009$	FCRAO
GMC Averages	$0.014 \pm 0.020^{\text{e}}$	$0.013 \pm 0.020^{\text{e}}$	

<sup>a</sup>Uncertainties are  $\pm 0.02$  for all FCRAO GMC data, see § 3.1.3.

<sup>b</sup>The S269 HCN data and the Orion B CS data showed clear evidence for the systematic problems discussed in § 3.1.3.

<sup>c</sup>These results compare well with those in Appendix B of Helfer & Blitz 1993, where we calculated  $I_{\text{CS}}/I_{\text{CO}} = 0.008$  for Orion B and  $I_{\text{CS}}/I_{\text{CO}} = 0.010$  for the Rosette.

<sup>d</sup> $3\sigma$  upper limits.

<sup>e</sup>See § 3.1.3 and footnote 7 for a discussion of the uncertainties.

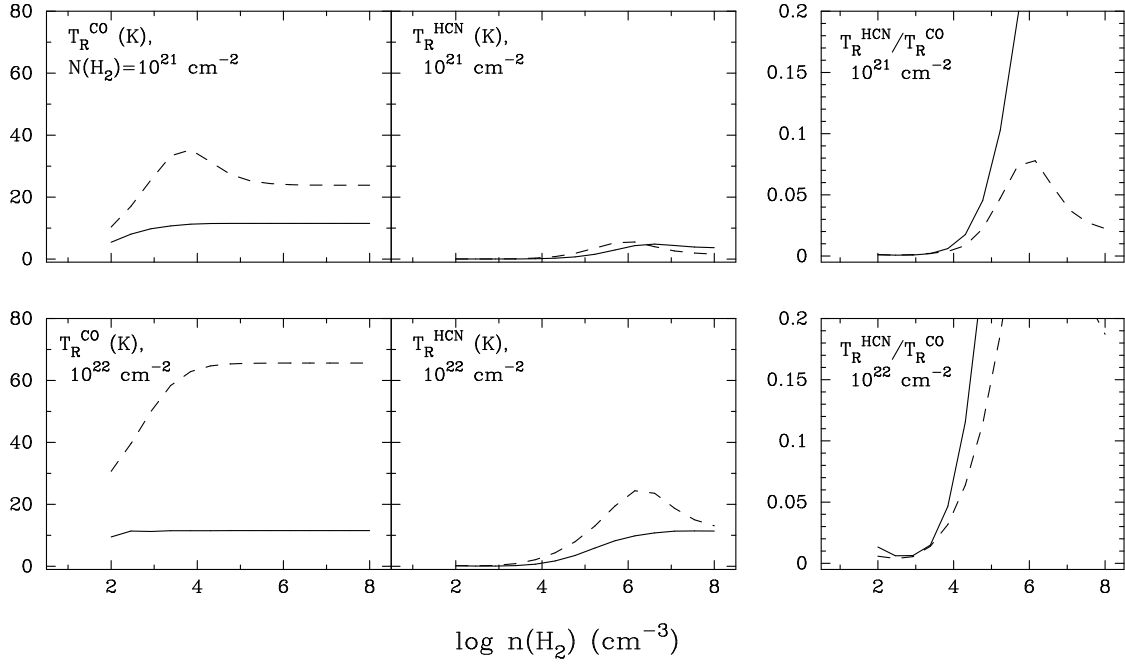


Fig. 1.— Results from sample LVG calculations of CO and HCN line excitation. Shown are results for the  $J = 1 - 0$  transitions only. The solid lines are for  $T_K = 15$  K, and the dashed lines are for  $T_K = 70$  K. The calculations assume  $[\text{HCN}]/[\text{CO}] = 10^{-4}$  and  $[\text{CO}]/[\text{H}_2] = 8 \times 10^{-5}$ . The top row is for  $N(\text{H}_2) = 1.3 \times 10^{21} \text{ cm}^{-2}$ , and the bottom is for  $N(\text{H}_2) = 1.3 \times 10^{22} \text{ cm}^{-2}$ . The left panels show the CO radiation temperature in K, the middle panels show the HCN radiation temperature in K, and the right panels show the ratio of the radiation temperatures  $T_R(\text{HCN})/T_R(\text{CO})$ .

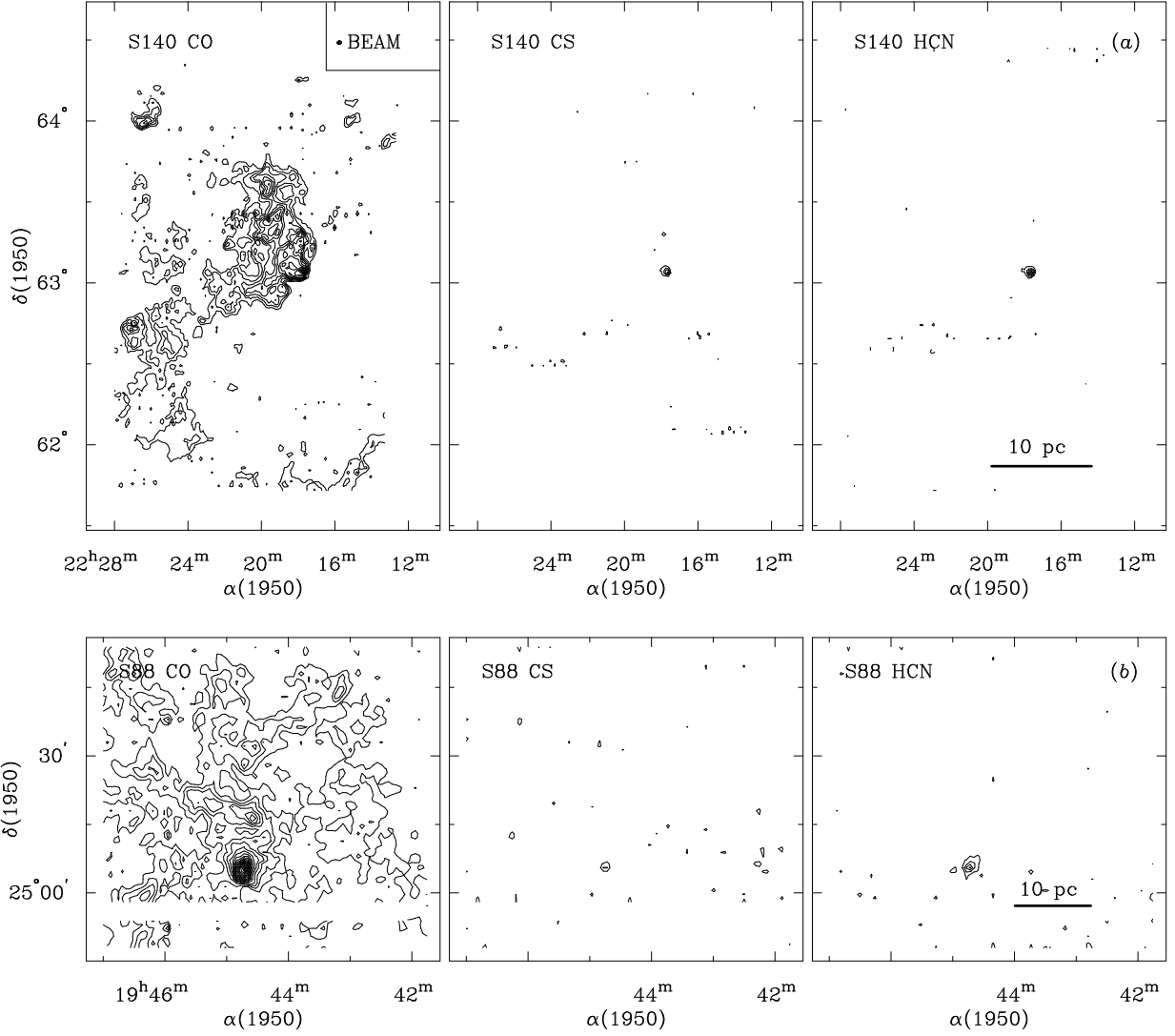


Fig. 2.— (a) CO, CS, and HCN emission from the GMC S140. The maps were made using the QUARRY multibeam receiver at the FCRAO 14 m telescope. Each map comprises some 23000 spectra. The  $1'$  resolution of the observations is shown in the upper right corner of the CO map, and the characteristic size scale of 10 pc is shown on the HCN map. The CO contour levels are  $\pm 5, 10, 15 \dots$  K km s $^{-1}$ , and the CS and HCN contours are  $\pm 3, 6, 9 \dots$  K km s $^{-1}$ . The 3 K km s $^{-1}$  contours some  $\sim 15'$  to the north of the peak on the CS and HCN maps show real emission in their spectra; all of the 3 K km s $^{-1}$  contours farther than  $\sim 15'$  away from the peak position on the CS and HCN maps are consistent with noise. The CO map is courtesy of Mark Heyer. (b) Same for S88. The CO and CS contours are as above; the HCN contours are  $\pm 3.3, 6.6, 9.9, \dots$  K km s $^{-1}$ .

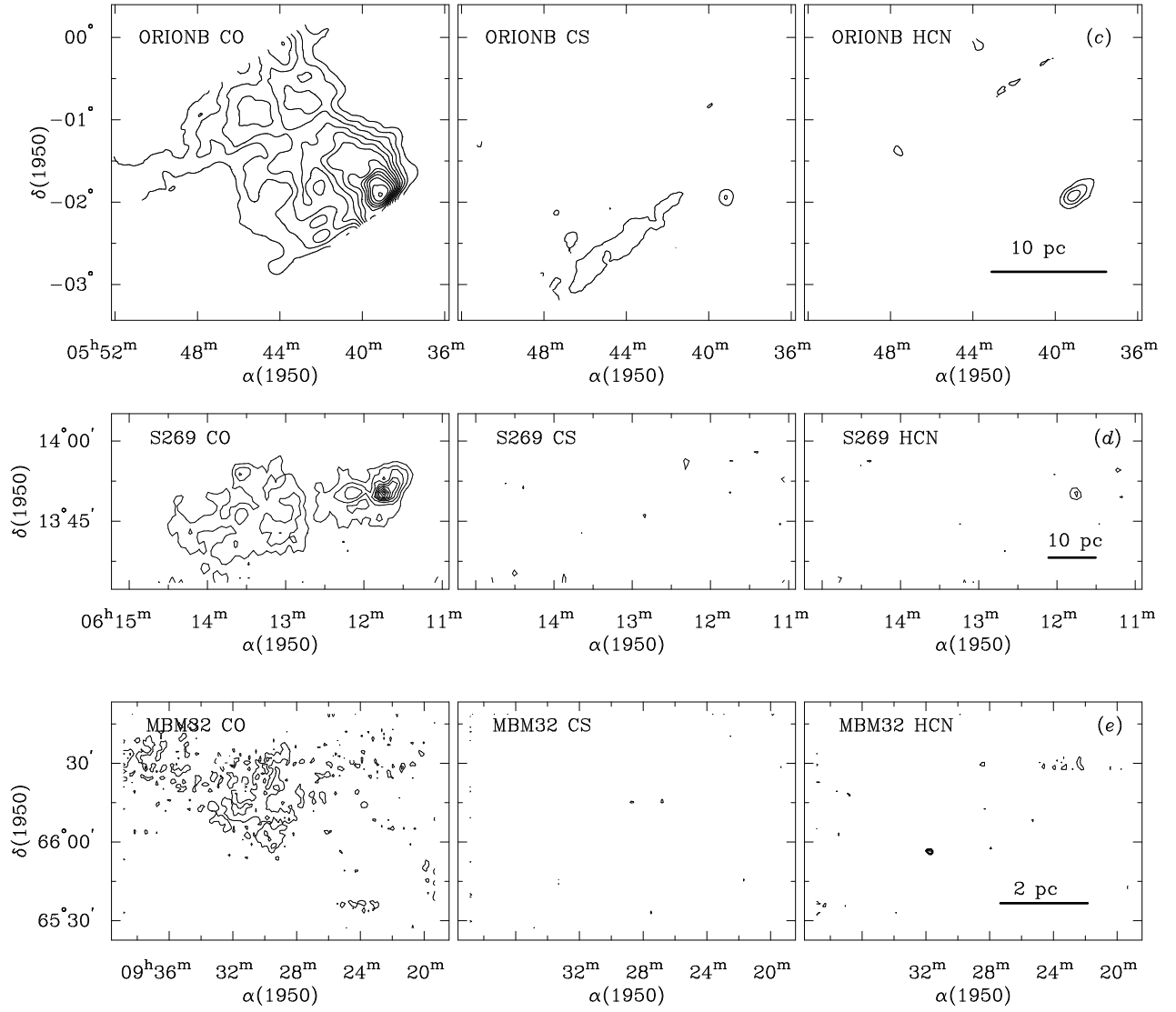


Fig. 2 continued.— (c) Same for Orion B. The CO contours are as above; the CS contours are  $\pm 1.5, 3, 4.5 \dots \text{K km s}^{-1}$ ; and the HCN contours are  $\pm 2.1, 4.2, 6.3 \dots \text{K km s}^{-1}$ . (d) Same for S269. The CO contours are as above; the CS contours are  $\pm 2.4, 4.8, 7.2 \dots \text{K km s}^{-1}$ ; and the HCN contours are  $\pm 2.1, 4.2, 6.3 \dots \text{K km s}^{-1}$ . (e) Same for MBM32. The CO contours are  $\pm 3, 6, 9 \dots \text{K km s}^{-1}$ ; the CS contours are  $\pm 1.2, 2.4, 3.6 \text{ K km s}^{-1}$ ; and the HCN contours are  $\pm 2.1, 2.8, 3.5 \dots \text{K km s}^{-1}$ .

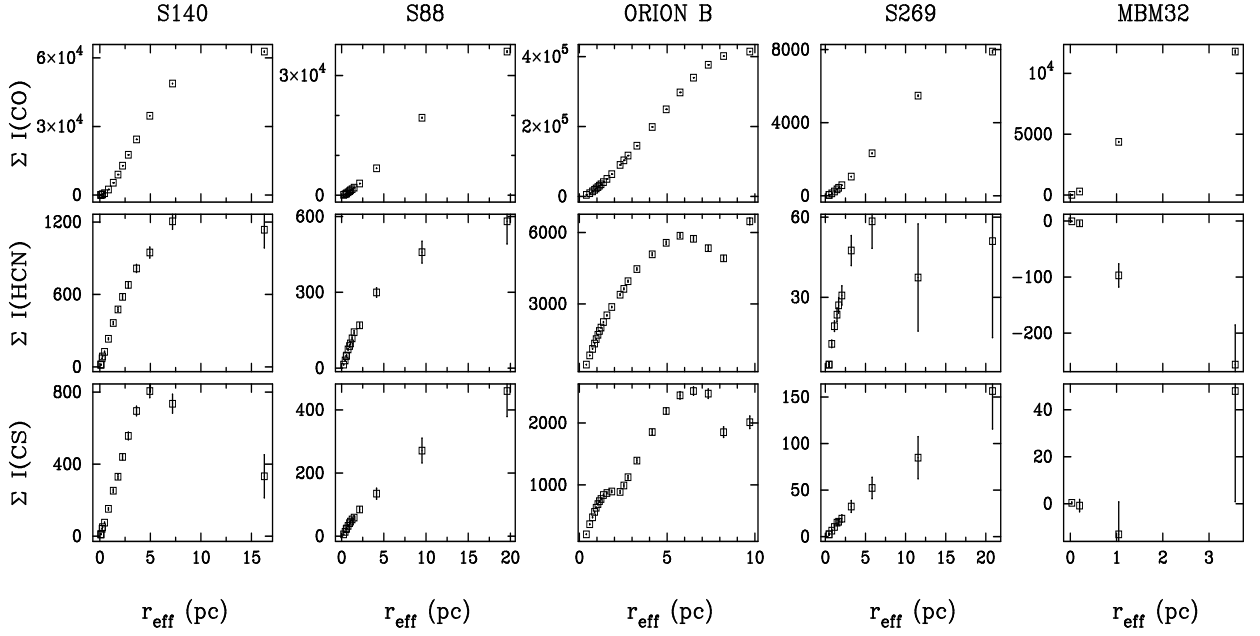


Fig. 3.— The summed intensities  $\Sigma I(\text{CO})$ ,  $\Sigma I(\text{HCN})$ , and  $\Sigma I(\text{CS})$  as a function of effective radius in each of the five clouds observed with QUARRY. The units of the ordinates are  $\text{K km s}^{-1}$ . The error bars underestimate the systematic uncertainties in the ratios at  $r_{\text{eff}} \gtrsim 5$  pc (see text).

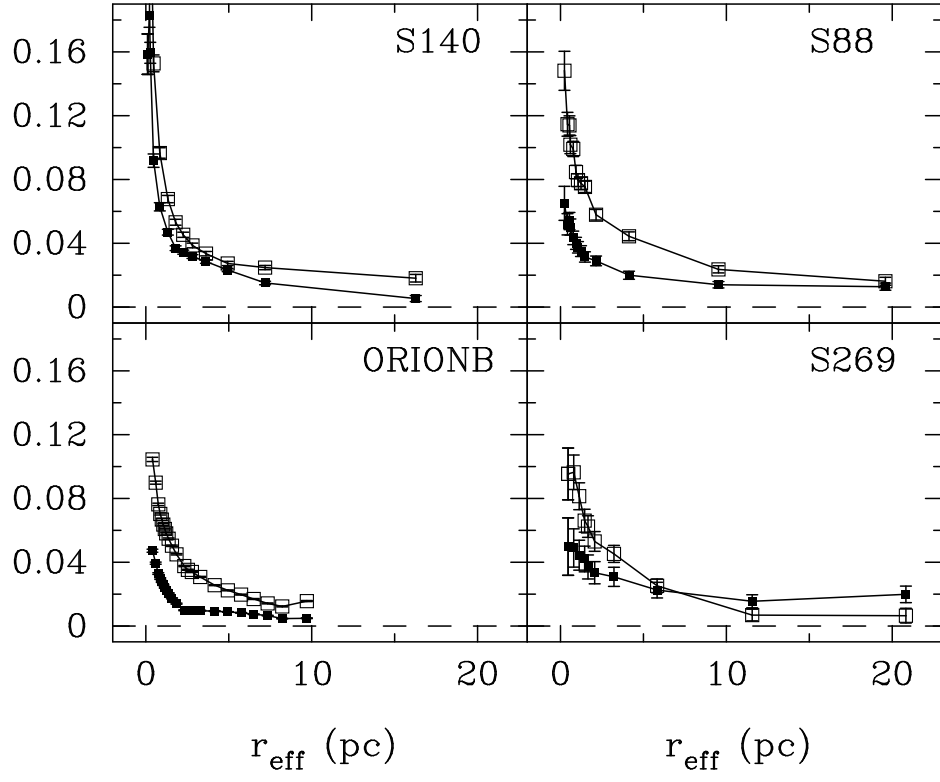


Fig. 4.— The integral ratios  $I_{\text{HCN}}/I_{\text{CO}}$  (open squares) and  $I_{\text{CS}}/I_{\text{CO}}$  (filled squares) as a function of effective radius in each of four GMCs measured with QUARRY. The error bars underestimate the systematic uncertainties in the ratios at  $r_{\text{eff}} \gtrsim 5$  pc (see text).

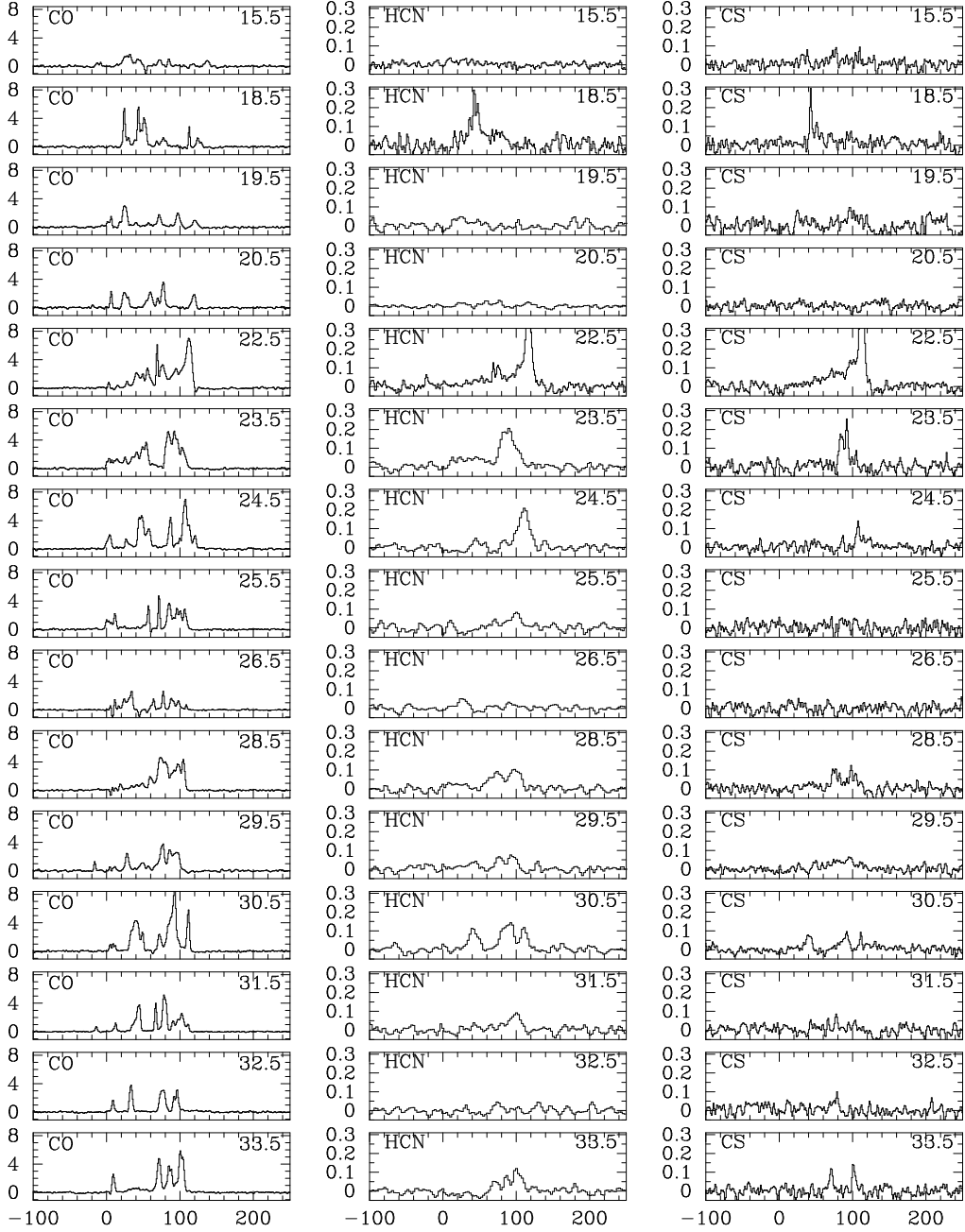


Fig. 5.— CO, HCN, and CS spectra from NRAO 12 m plane survey. The longitude is given in the upper right corner of each spectrum. The abscissa is  $v_{\text{LSR}}$  in  $\text{km s}^{-1}$ , and the ordinate is  $T_{\text{R}}^*$  in K. Note that the HCN and CS spectra have a different temperature scale than the CO spectra.

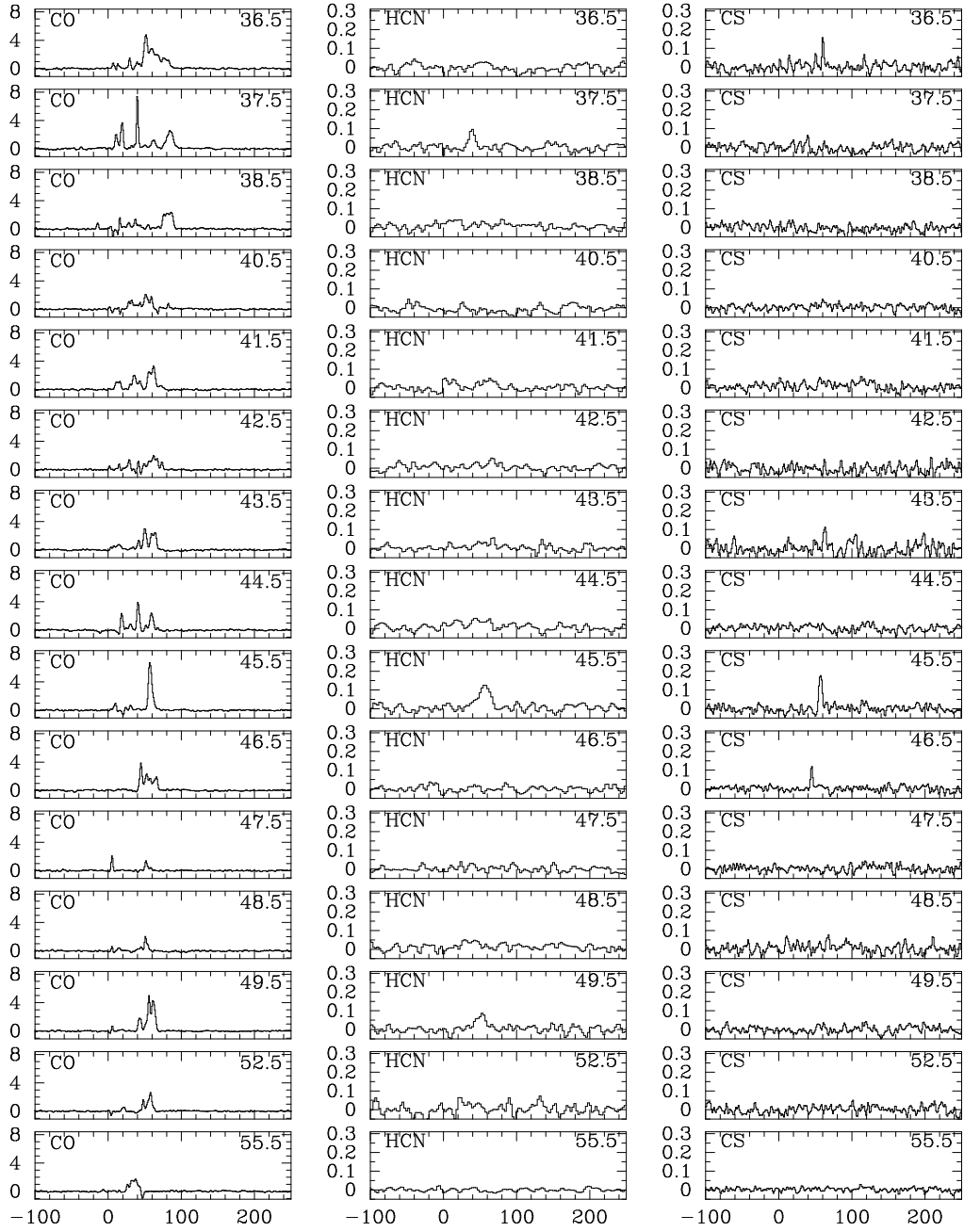


Fig. 5.— continued.

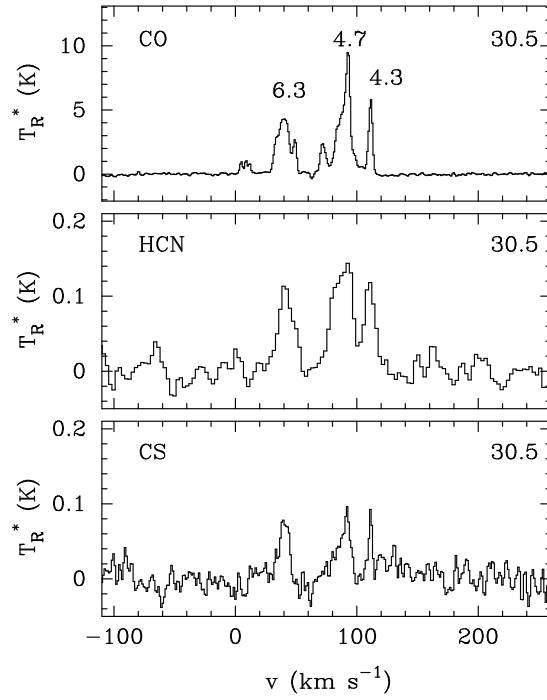


Fig. 6.— CO, HCN, and CS spectra from  $l = 30.5^\circ$ . The three strongest features in the CO spectrum are labeled with their Galactocentric distances in kpc.

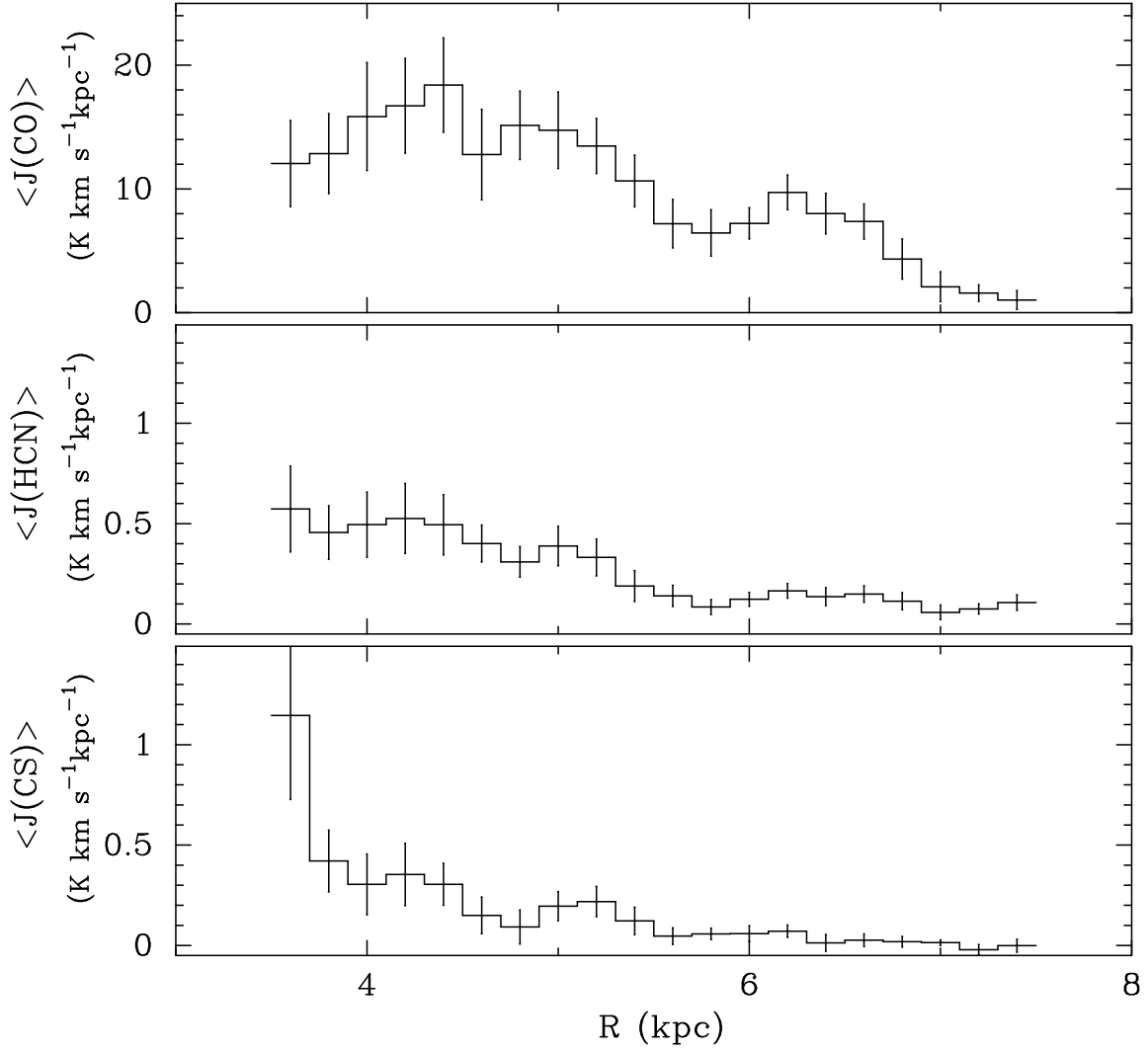


Fig. 7.— Radial distributions of CO, HCN, and CS emissivities in the plane of the Milky Way.

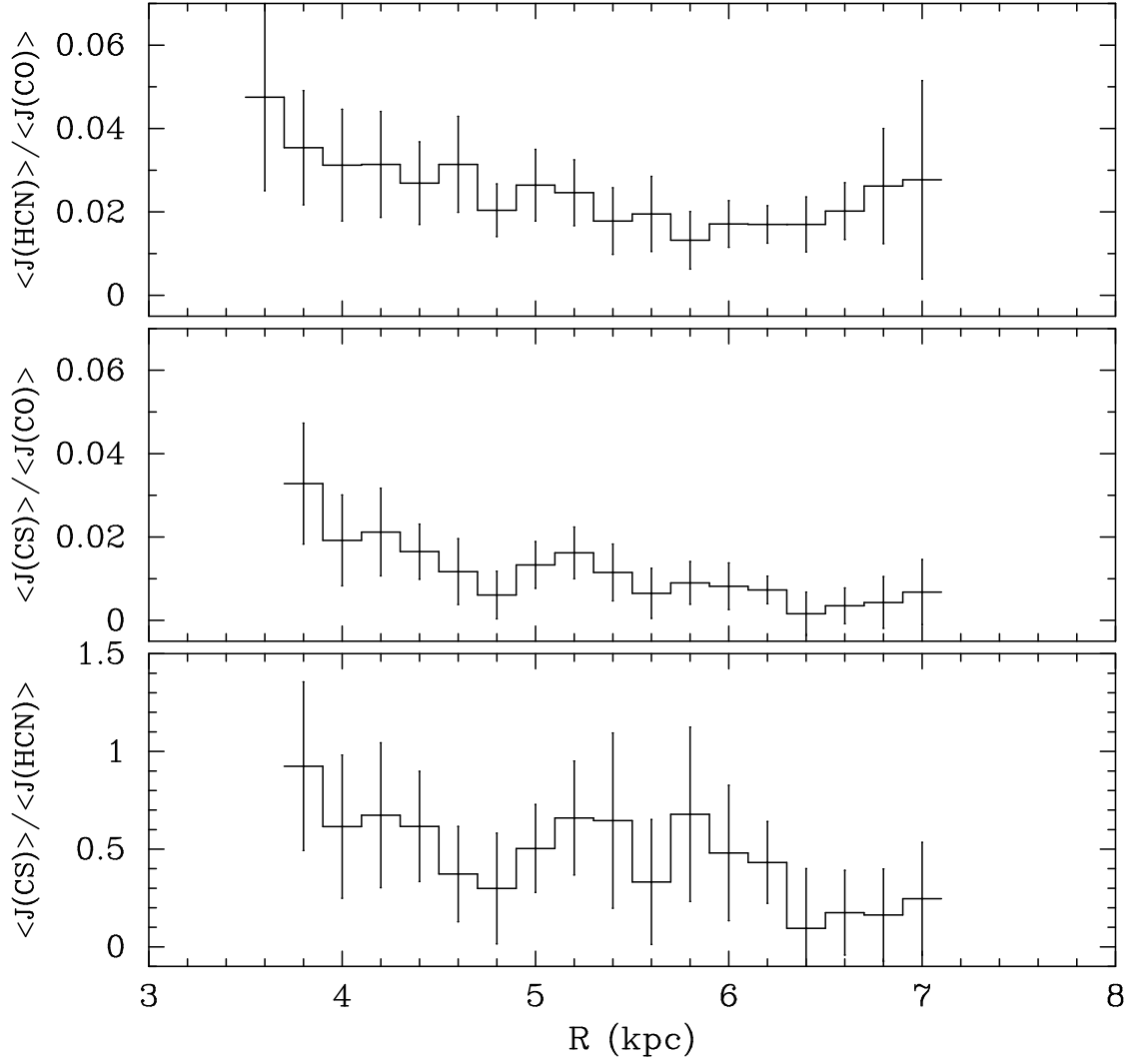


Fig. 8.— The ratios of HCN, CS, and CO emissivities as a function of radius in the plane of the Milky Way.

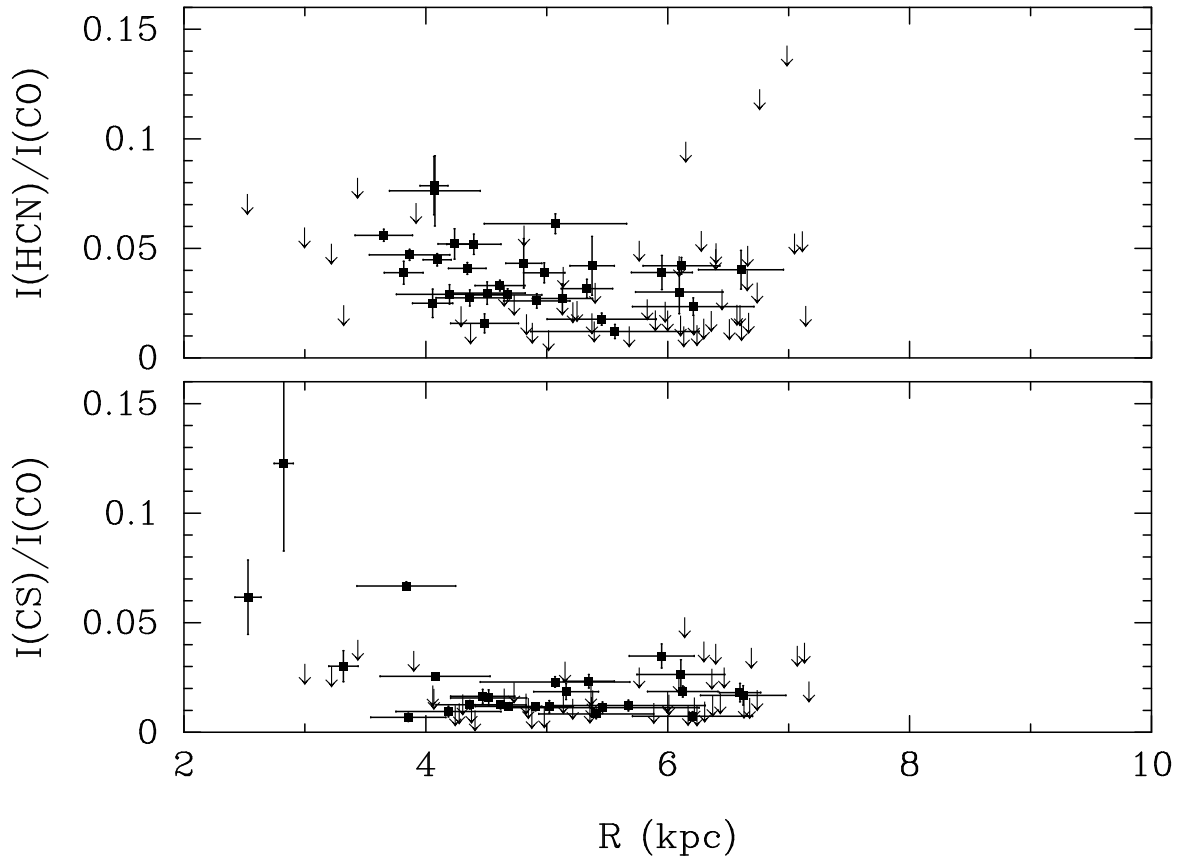


Fig. 9.— The dense gas ratios over individual Milky Way features. The arrows represent  $2\sigma$  upper limits, and the filled squares represent detected ratios. The vertical error bars are the  $1\sigma$  uncertainties in the ratios, and the horizontal lines represent the range of the Galactocentric radii implied by the velocity limits of each feature.

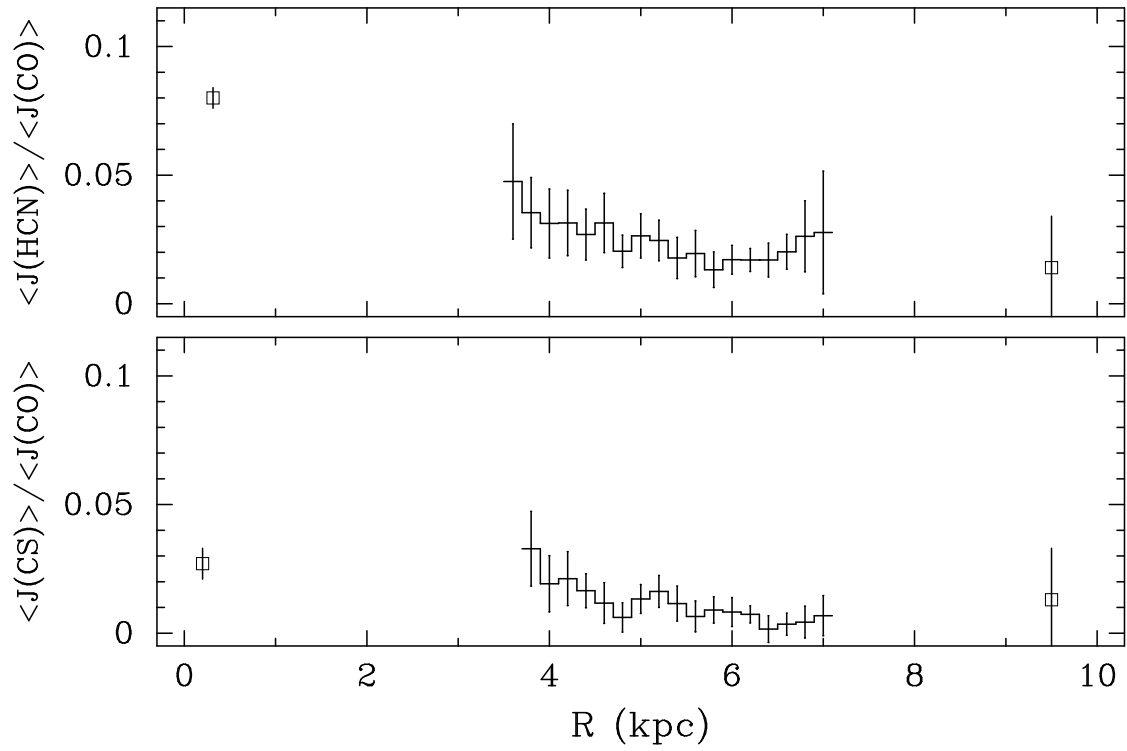


Fig. 10.— Dense gas ratios in the Milky Way. At  $R = 0.3$  kpc, the HCN/CO point is from Jackson et al. 1996, and the CS/CO point is from Helfer & Blitz 1993. The points shown at  $R = 9.5$  kpc represent the averages over the individual GMCs presented in this study; the clouds themselves are located at different directions and distances from the Sun.

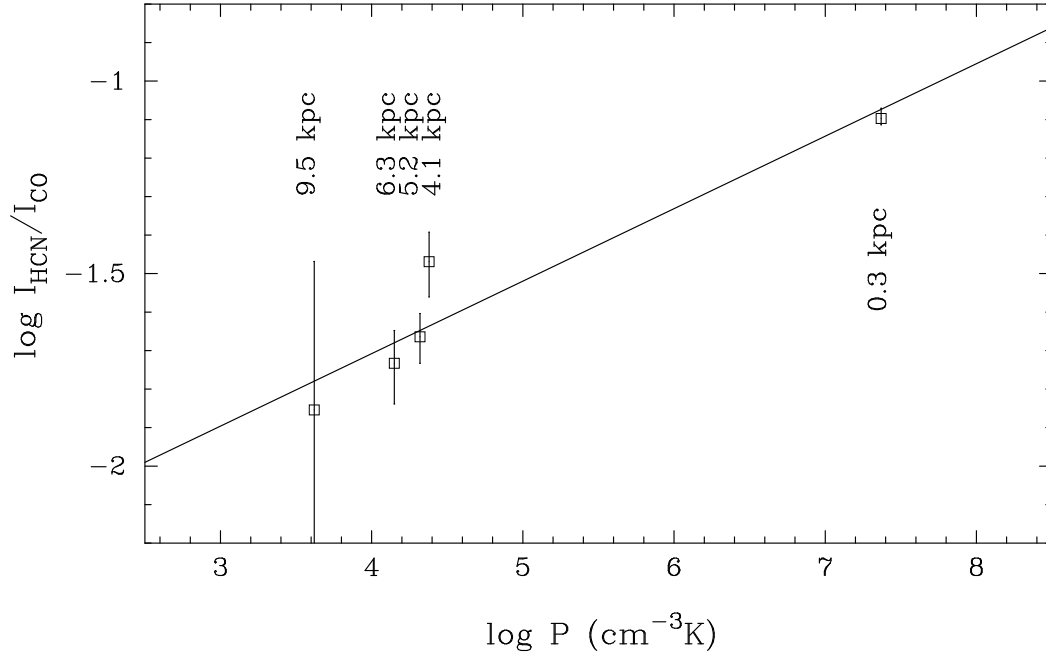


Fig. 11.— Dense gas ratios plotted against pressure in the Milky Way. Each point is labeled with its distance from the Galactic Center. The solid line is a linear least squares fit to the data.